





Statistics of topological defects across a phase transition in a superconducting quantum processor

Daniil Teplitskiy ^{1,*}, Oriël Kiss ^{1,2,*}, Michele Grossi ¹ and Antonio Mandarino ^{3,4,†}

¹*European Organization for Nuclear Research (CERN), Geneva 1211, Switzerland*

²*Department of Nuclear and Particle Physics, University of Geneva, Geneva 1211, Switzerland*

³*International Centre for Theory of Quantum Technologies,*

University of Gdańsk, Jana Bażyńskiego 1A, 80-309 Gdańsk, Poland

⁴*Department of Physics Aldo Pontremoli, Università degli Studi di Milano, Via Celoria 16, 20133 Milano, Italy*

(Dated: October 10, 2024)

When a quantum phase transition is crossed within a finite time, critical slowing down disrupts adiabatic dynamics, resulting in the formation of topological defects. The average density of these defects scales with the quench rate, adhering to a universal power law as predicted by the Kibble-Zurek mechanism (KZM). In this study, we aim to investigate the counting statistics of kink density in the 1D transverse-field quantum Ising model. We demonstrate on a 20-qubit quantum processing unit, that higher-order cumulants follow a universal power law scaling as a function of the quench time. We also show the breakdown of the KZM mechanism for short quenches for finite-size systems. Tensor network simulations corroborate our quantum simulation results for bigger systems not in the asymptotic limit.

Introduction.— The Kibble-Zurek mechanism (KZM) is a fundamental theory in nonequilibrium statistical physics, widely used to describe the dynamics of systems undergoing continuous phase transitions. Initially motivated by cosmological considerations regarding structure formation in the early Universe [1], Kibble’s pioneering work laid the groundwork for Zurek to extend these ideas to superfluid helium [2], paving the way to cosmological experiments via simulation in acoustic analogues. According to the KZM, when a system is driven across a phase transition, by varying a (or a set of) time-dependent control parameter $h(t)$ which crosses its critical value h_c within a finite quench time τ_Q , it cannot remain in equilibrium due to the critical slowing down phenomenon [3, 4].

At the critical point h_c , systems showing a second-order phase transition exhibit a null mass gap or a divergent correlation length, therefore their ground state does not evolve any longer adiabatically [3, 5]. As the system approaches the critical point, the equilibrium relaxation time diverges, preventing the system from adapting quickly enough to remain in equilibrium. This results in non-adiabatic dynamics, leading to the formation of excitations such as topological defects. These defects, which form at the boundaries between independently developed domains—each selecting different broken symmetries—are robust remnants of the original symmetries.

The KZM predicts a universal scaling law for the mean value of the density of defects, n , as a function of the quench time, namely $n \propto \tau_Q^{-\alpha}$. The exponent α is determined by the system’s geometry and by the two critical exponents z and ν , the dynamical and correlation length ones respectively, such that the logarithm of the mass

gap scales as the product of the two. This scaling behavior has been confirmed in both classical and quantum systems, making the KZM a robust tool for analyzing nonequilibrium dynamics [6, 7].

In the quantum realm, the KZM has been validated in systems undergoing quantum phase transitions, such as the transverse field quantum Ising model in one dimension (TFQIM), for which the exact dynamics of a quantum phase transition was analytically derived and explained in terms of a series of Landau-Zener transitions [8]. The peculiarities of such systems are that in contrast to the original cosmological derivation and its superfluid analog, here the underlying symmetry is discrete (\mathbf{Z}_2), and a unitary dissipation-free evolution leads to a non-equilibrium configuration where all cumulants—not just the first one (the mean)—of the probability distribution of the topological defects exhibit a KZM-like scaling. Del Campo and collaborators have shown that in the thermodynamical limit the full counting statistics of kinks in TFQIM reveal universal behavior for slow enough quenches [9] and a breakdown of the KZM-scaling with a kink formation dynamics independent on τ_Q , i.e., a constant defect density, for fast quench [10]. In addition, they measured and determined the biases caused by symmetry breaking [11] and the deviations that occur around equilibrium [12]. Although the previous work was conducted analytically on systems with one dimension, Schmitt *et al.* [13] investigated the KZM in two-dimensional systems using numerical techniques.

Experiments probing the KZM have been conducted across a variety of platforms, including ultracold gases [14], Rydberg atoms [6], trapped ions [7] and both analog [15] and digital [16] quantum devices based on superconducting qubits. These experiments often involve measuring the statistical properties of topological defects formed during the phase transition, providing empirical support for the KZM and its broader implications in statistical physics. Ultimately, the KZM remains a cornerstone the-

* These authors contributed equally to this work.

† antonio.mandarino.work@gmail.com

ory, offering a quantitative framework for understanding the formation of topological defects and the dynamics of symmetry breaking in a wide range of physical systems.

Digital quantum computing is rapidly becoming a promising approach for many-body quantum simulations, offering the ability to efficiently perform highly precise computations on large systems. Although asymptotically optimal methods, based on quantum signal processing [17], hold significant potential, they require substantial advancements in quantum error correction [18, 19] and quantum hardware capabilities. Nonetheless, recent experiments, have successfully demonstrated the practical utility of digital quantum computing [20–24], using instead quantum error mitigation [25] strategies. These experiments bridge the gap towards a fault-tolerant paradigm, by pushing the capabilities of current quantum devices.

Here we report an experimental confirmation of the KZM for the cumulants of the kink density distribution via simulation on the 20-qubit digital quantum processing unit based on superconducting transmon qubits IQM Garnet [26].

The Model.— The one-dimensional transverse-field quantum Ising model is a paradigmatic system in the study of quantum phase transitions and critical phenomena. It consists of a linear chain of spins, each governed by two competing interactions: a transverse field and nearest-neighbor coupling. We consider the TFQIM of the form

$$H(t) = -J(t) \sum_{i=1}^{N-1} X_i X_{i+1} - h(t) \sum_{i=1}^N Z_i \quad (1)$$

with $J(t) = J_0 t / \tau_Q$ and $h(t) = (1 - t / \tau_Q) h_0$. The competition between these interactions drives a quantum phase transition at a critical field strength $h_c / J_c = 1$, where the system undergoes a transition from a ferromagnetic phase, characterized by ordered spin alignment, to a paramagnetic phase, where the spins are aligned with the transverse field. The model is exactly solvable, making it a cornerstone for understanding quantum criticality and non-equilibrium dynamics in low-dimensional systems. We fix $h_0 = J_0 = 1$ such that the quantum phase transition is crossed at the middle of the quench, i.e. at $t = \tau_Q / 2$. The initial state is chosen as the ground state at $t = 0$, and takes the form of the all spin up state $|0\rangle^{\otimes N} \equiv |\bar{0}\rangle$. To measure the number of topological defects we consider the kink operator

$$\hat{n} = \frac{1}{2N} \sum_{i=1}^{N-1} (\mathbb{1} - X_i X_{i+1}). \quad (2)$$

The cumulants are the coefficients of the series expansion of the moment-generating function of the kink distributions, in the quantum simulation we focus on the

first three, namely:

$$\kappa_1 = \langle \hat{n} \rangle, \quad \kappa_2 = \langle (\hat{n} - \langle \hat{n} \rangle)^2 \rangle = \langle \hat{n}^2 \rangle - \kappa_1^2 \quad (3)$$

$$\kappa_3 = \langle (\hat{n} - \langle \hat{n} \rangle)^3 \rangle = \langle \hat{n}^3 \rangle - 3\kappa_1\kappa_2 - \kappa_1^3 \quad (4)$$

This operator can be estimated up to error ϵ by measuring the wavefunction in the Hadamard basis at least $\text{Var}[\hat{n}^k] / \epsilon^2 \leq 1 / \epsilon^2$ times. All the correlators can be measured in this basis and can therefore be estimated simultaneously. The main challenge arises for long quench times, since the expectation values are expected to be small, and thus require a higher number of measurements to be detected from statistical noise. However, there is no fundamental problem in estimating expectation values in this way.

Time-dependent Hamiltonian simulation.— The quench is performed by evolving the initial state under a time-dependent Hamiltonian $H(t)$. The time evolution is obtained via the time-ordered unitary evolution stemming from the Hamiltonian as

$$\mathcal{U}(t_f, t_0) = \mathcal{T} \exp \left(-i \int_{t_0}^{t_f} H(t) dt \right), \quad (5)$$

where \mathcal{T} is the time ordering operator to account for the non-commutativity at different time $[H(t), H(t')] \neq 0$. There exist different ways of implementing $\mathcal{U}(t_f, t_0)$ on digital quantum computers, the most straightforward being the quasistatic approximation [27]. In this framework, the simulation time is sliced into r Trotter steps of size $\Delta t = (t_f - t_0) / r$, in which $H(t) \approx H(k' \Delta t)$, for $k' = k + 1/2$ and $t \in [k \Delta t, (k+1) \Delta t]$. The time-evolution operator can thus be approximated by

$$\mathcal{U}(t_f, t_0) \approx \prod_{k=1}^r \exp[-i \Delta t H(t_0 + k' \Delta t)]. \quad (6)$$

The matrix exponential $\exp(-i \Delta t H)$ is not directly implementable on a digital quantum processor. Therefore, we decompose it into fundamental quantum gates [28], e.g., using the Trotter-Suzuki product-formula (PF) [29], whose error scales polynomial in time, and pre-factor depending on the commutators [30]. For simplicity, let us assume that the Hamiltonian breaks down into two groups of pairwise commuting term,

$$H(t) = f(t)A + g(t)B, \quad (7)$$

such that $\exp(iA)$ and $\exp(iB)$ are exactly implementable. We use a second-order product formula, which is given in the static case by

$$\exp(-iHt) \approx \exp(-iAt/2) \exp(-iBt) \exp(-iAt/2). \quad (8)$$

Merging both approximations (6) and (8), we obtain

$$\begin{aligned} \mathcal{U}(t) &\equiv \mathcal{U}(t_f = t, t_0 = 0) \\ &= \prod_{k=1}^r \exp[-if(k' \Delta t)A \Delta t / 2] \\ &\quad \cdot \exp[-ig(k' \Delta t)B \Delta t] \exp[-if(k' \Delta t)tA \Delta t / 2]. \end{aligned} \quad (9)$$

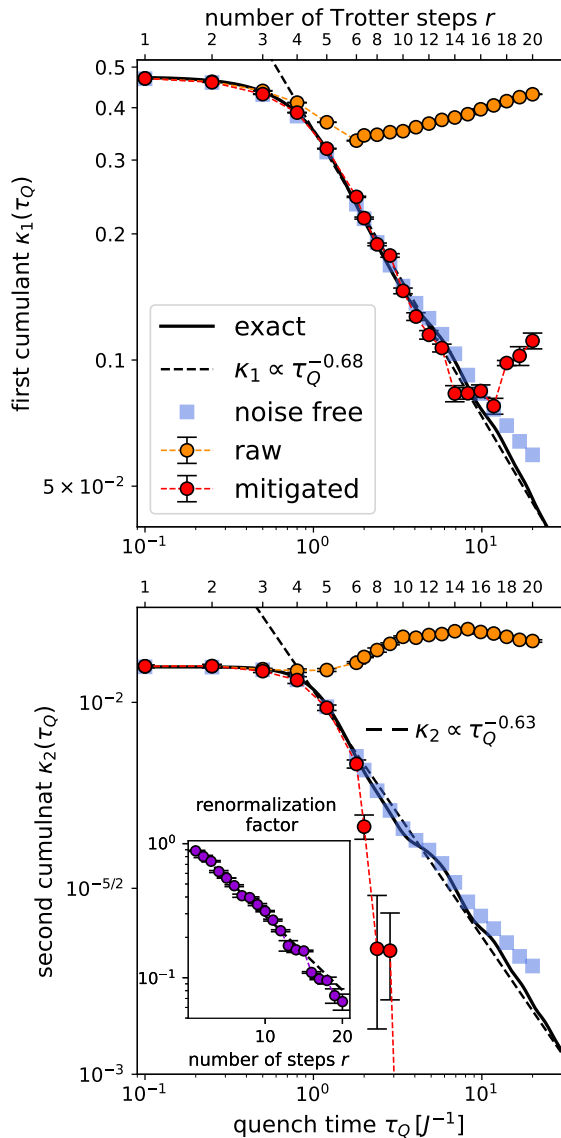


Figure 1: **Quantum simulation on IQM Garnet** ($N = 19$). The two first cumulants of the kink density are shown as a function of the quench time, as well as the number of Trotter steps. The blue squares denote noise free simulation, the orange points the raw data and the red the results obtained after the full pipeline of error mitigation. The complexity of the circuits is increased as one additional Trotter steps per data point. The black continuous line shows the exact evolution, while the decay rate appears as a dotted-line. The inset shows the renormalization factor (purple) as a function of the circuit’s depth.

Straightforward extensions of the quasistatic PF method include adaptive step sizing [31], random compilation techniques like QDrift [32, 33] with one-norm scaling [34], and leveraging the interaction picture [35]. While asymptotically superior methods exist—such as those based on the Dyson series [36], Magnus expansions

[37, 38], discrete clocks [39], or flow equations [40]—the PF method is notably effective in practice, especially for systems with a high degree of locality [41].

Quantum simulation.— In this section, we report numerical experiments, both with quantum hardware and tensor networks, of the correlation’s decay across the quantum phase transition.

We begin by performing the quench on the IQM Garnet superconducting quantum computer [26], which consists of twenty transmon qubits and achieves a two-qubit gate fidelity of 99.5% [42]. Due to the chip’s connectivity, we work with a system of $N = 19$ spins. We implement the second-order PF method, varying the number of Trotter steps r up to 20 across different quench times $\tau_Q \in [0.1, 20]$. The first two cumulants are presented in Fig. 1, with noise-free simulations shown as blue squares, raw data as purple dots, and error-mitigated results as red dots. The continuous line represents a near-exact evolution, approximated using 2000 Trotter steps. Higher-order moments are not displayed, as they are several orders of magnitude smaller and would require significantly more measurements to be accurately estimated.

Error mitigation is applied using noise renormalization techniques [22, 24, 43–45], along with 50 instances each of Pauli [46] and readout [47] twirling, and matrix-free measurement mitigation [48]. We normalize each expectation value by taking advantage of the identity

$$\langle \bar{\mp} | \mathcal{U}^\dagger(t) \hat{n} \mathcal{U}(t) | \bar{\mp} \rangle = 1, \quad (10)$$

where we use the mitigating scheduling function $h(t) = \pi/\Delta t$ for the field, such that the corresponding evolution becomes a symmetry of the Hamiltonian. We observe that the renormalization factor decays exponentially fast with the depth, as shown in the inset of the lower plot of Fig. 1. Therefore, this process can not be applied for arbitrary depth circuit, but in this case it enables us to extend it by a factor four. Each circuits is run 2000 times and the error bars correspond to a 99% confidence interval computed via Bayesian data augmentation. The accuracy limit resulting from finite statistics is $10^{-5/2}$, is depicted on the corresponding axis. For completeness, all of these methods are described in the appendices A and B.

To support our findings on finite-size systems, we conduct numerical experiments using matrix-product states (MPS) [49] with larger spin systems to approximate results obtained in the thermodynamic limit [9].

We begin by calculating the decay rate α as a function of system size by fitting the data to a model of the form $\propto \tau_Q^{-\alpha}$, in line with the decay predicted by the KZM. For this analysis, we perform MPS simulations with a fixed error tolerance of 10^{-10} , based on which the smallest coefficients (from the singular value decomposition) with a lower sum of their squares than this are discarded, and 300 Trotter steps, extracting the decay rate using 10^5 shots per run. As previously mentioned, expectation values tend to be small for higher-order cumulants. Therefore, our focus lies on the first three cumulants. We show

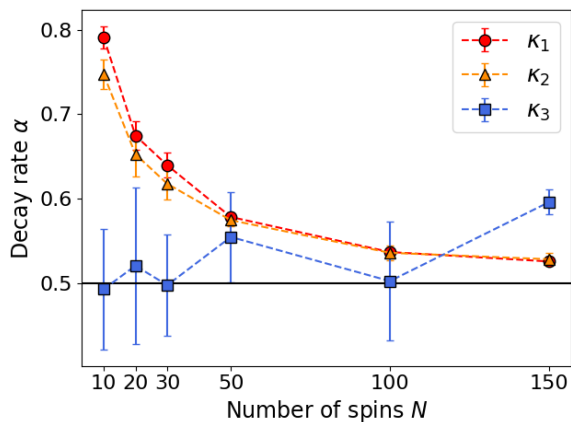


Figure 2: **Decay rate scaling.** The decay rate α of the three first cumulants (red, orange and blue respectively) extracted by least-square regression is shown as a function of the system size. The simulations are performed using MPS at fixed error threshold of 10^{-10} . The error bars correspond to one standard deviation due to the finite statistics. We observe that all decay rates approaches $1/2$ (continuous black line), as predicted by the theory in the thermodynamic limit.

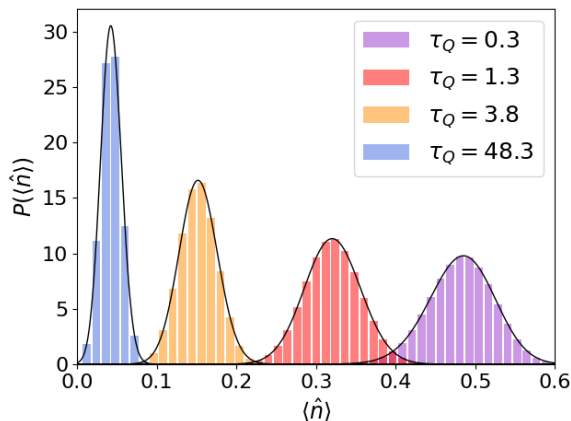


Figure 3: **Distribution of the kink density.** The probability distribution function $P(\langle \hat{n} \rangle)$ of the kink density is shown as a function of different quench time (colors). The simulation is performed using MPS on $N = 150$ spins.

in Fig. 2 that the decay rate for the first three cumulants approaches $1/2$. The uncertainty on higher cumulants increases, due to statistical noise.

Finally, we reconstruct the kink probability distribution $P(\langle \hat{n} \rangle)$ from the first three moments at fixed system size $N = 150$ for different quench times by using the maximum entropy method [50], which is shown in Fig. 3. We observe that the probability distributions become narrower, and the expectation value of the kink density decreases with longer quench times, consistent

with the decay rate of $1/2$ observed across all cumulants, which is consistent with the analytical predictions of del Campo [9].

Discussions. - Simulations of the critical dynamical behavior till a few years ago were only able in suitably designed laboratories. Anyway, the advent of on-demand quantum digital processing units made testing the universality of scaling laws (and their deviations) in complex systems possible for a much broader number of researchers. We perform a quantum simulation of the dynamics of a quantum phase transition using a digital superconducting quantum computer, with a circuit's depth of up to one hundred sequential CNOT gates, employing a variety of error mitigation techniques. Using error mitigation, we increase the number of reliable Trotter steps by a factor of four, at least for the first cumulant. Computing higher cumulants requires more statistics, as they are typically order of magnitude lower. Although the cost of error mitigation generally increases exponentially with the level of noise [51–53], making it unsustainable in the long term, we argue that it remains a vital tool for utilizing quantum computers before achieving full fault-tolerance. Specifically, we contend that error mitigation bridges the gap towards the era of early fault-tolerance [54] and facilitates the implementation of typical algorithms [55–57] of this era.

We have empirically demonstrated in a finite-size TFQIM the deviations from the KZM during rapid quenches across a continuous phase transition. These deviations lead to a breakdown in the predicted power-law scaling of defect density with τ_Q , resulting in a plateau preceding the $\tau_Q^{-\alpha}$ typical scaling. Additionally, we have shown how the distribution of the density of topological defects follows a binomial distribution, nearly Gaussian when the central limit theorem requirements are met [12]. This model predicts that higher-order cumulants of the defect distribution scale with the quench time in a universal manner. These findings follow the pioneer line suggested by Del Campo [10, 58] to test the counting statistics of topological defects and the corresponding breakdown in experimental systems. We investigated finite-size effects using MPS by analyzing the decay rate as a function of system size, as well as recovering the full probability distribution. We observed that the decay rate converges to $1/2$ for the first three cumulants, approaching the value predicted in the thermodynamic limit and in pure coherent dynamics.

Our work goes in the direction of testing the scaling laws in quantum critical phenomena and has broad relevance in nonequilibrium statistical mechanics, numerically proving KZM, and the breakdown of adiabatic dynamics, for the statistics of the kink-density in a TFQIM. We surmise our findings are of interest to better understand the validity of quantum simulation and quantum annealing [16], and the study of critical and thermalization phenomena in non-dissipative systems [5, 15].

ACKNOWLEDGMENTS

The authors thank IQM for providing access to their devices. O.K. and M.G. are supported by CERN through the CERN Quantum Technology Initiative. A.M. acknowledges the project CQES of the Italian Space Agency (ASI) for having partially supported this research (grant N. 2023-46-HH.0).

AUTHOR CONTRIBUTIONS

O.K. and D.T. contributed equally to this work. A.M. designed the study. O.K. carried out the quantum simulation, while D.T. executed the tensor networks calculations. O.K. and A.M. wrote the manuscript with inputs from all authors. M.G. and A.M. supervised and coordinated the project.

-
- [1] T. Kibble, Some implications of a cosmological phase transition, *Physics Reports* **67**, 183 (1980).
- [2] W. H. Zurek, Cosmological experiments in superfluid helium?, *Nature* **317**, 505 (1985).
- [3] J. Dziarmaga, Dynamics of a quantum phase transition and relaxation to a steady state, *Advances in Physics* **59**, 1063 (2010).
- [4] A. Del Campo and W. H. Zurek, Universality of phase transition dynamics: Topological defects from symmetry breaking, *International Journal of Modern Physics A* **29**, 1430018 (2014).
- [5] A. Polkovnikov, K. Sengupta, A. Silva, and M. Vengalattore, Colloquium: Nonequilibrium dynamics of closed interacting quantum systems, *Rev. Mod. Phys.* **83**, 863 (2011).
- [6] A. Keesling, A. Omran, H. Levine, H. Bernien, H. Pichler, S. Choi, R. Samajdar, S. Schwartz, P. Silvi, S. Sachdev, P. Zoller, M. Endres, M. Greiner, V. Vuletić, and M. D. Lukin, Quantum Kibble-Zurek mechanism and critical dynamics on a programmable rydberg simulator, *Nature* **568**, 207 (2019).
- [7] J.-M. Cui, F. J. Gómez-Ruiz, Y.-F. Huang, C.-F. Li, G.-C. Guo, and A. del Campo, Experimentally testing quantum critical dynamics beyond the Kibble-Zurek mechanism, *Communications Physics* **3**, 44 (2020).
- [8] J. Dziarmaga, Dynamics of a quantum phase transition: Exact solution of the quantum Ising model, *Phys. Rev. Lett.* **95**, 245701 (2005).
- [9] A. del Campo, Universal statistics of topological defects formed in a quantum phase transition, *Phys. Rev. Lett.* **121**, 200601 (2018).
- [10] H.-B. Zeng, C.-Y. Xia, and A. del Campo, Universal breakdown of Kibble-Zurek scaling in fast quenches across a phase transition, *Phys. Rev. Lett.* **130**, 060402 (2023).
- [11] M. M. Rams, J. Dziarmaga, and W. H. Zurek, Symmetry breaking bias and the dynamics of a quantum phase transition, *Phys. Rev. Lett.* **123**, 130603 (2019).
- [12] F. Balducci, M. Beau, J. Yang, A. Gambassi, and A. del Campo, Large deviations beyond the Kibble-Zurek mechanism, *Phys. Rev. Lett.* **131**, 230401 (2023).
- [13] M. Schmitt, M. M. Rams, J. Dziarmaga, M. Heyl, and W. H. Zurek, Quantum phase transition dynamics in the two-dimensional transverse-field Ising model, *Science Advances* **8**, eabl6850 (2022).
- [14] I.-K. Liu, J. Dziarmaga, S.-C. Gou, F. Dalfovo, and N. P. Proukakis, Kibble-Zurek dynamics in a trapped ultracold bose gas, *Phys. Rev. Res.* **2**, 033183 (2020).
- [15] T. I. Andersen, N. Astrakhantsev, A. Karamlou, J. Berndtsson, J. Motruk, A. Szasz, J. A. Gross, T. Westerhout, Y. Zhang, E. Forati, *et al.*, Thermalization and criticality on an analog-digital quantum simulator (2024), [arXiv:2405.17385](https://arxiv.org/abs/2405.17385) [quant-ph].
- [16] A. Miessen, D. J. Egger, I. Tavernelli, and G. Mazzola, Benchmarking digital quantum simulations and optimization above hundreds of qubits using quantum critical dynamics (2024), [arXiv:2404.08053](https://arxiv.org/abs/2404.08053) [quant-ph].
- [17] G. H. Low and I. L. Chuang, Optimal Hamiltonian simulation by quantum signal processing, *Phys. Rev. Lett.* **118**, 010501 (2017).
- [18] D. Bluvstein, S. J. Evered, A. A. Geim, S. H. Li, H. Zhou, T. Manovitz, S. Ebadi, M. Cain, M. Kalinowski, D. Hangleiter, J. P. B. Ataiades, N. Maskara, I. Cong, X. Gao, P. S. Rodriguez, T. Karolyshyn, G. Semeghini, M. J. Gullans, M. Greiner, V. Vuletić, and M. D. Lukin, Logical quantum processor based on reconfigurable atom arrays, *Nature* **626**, 58 (2024).
- [19] R. Acharya, L. Aghababaie-Beni, I. Aleiner, T. I. Andersen, M. Ansmann, F. Arute, K. Arya, A. Asfaw, N. Astrakhantsev, J. Atalaya, *et al.*, Quantum error correction below the surface code threshold (2024), [arXiv:2408.13687](https://arxiv.org/abs/2408.13687) [quant-ph].
- [20] Y. Kim, A. Eddins, S. Anand, K. X. Wei, E. van den Berg, S. Rosenblatt, H. Nayfeh, Y. Wu, M. Zaletel, K. Temme, and A. Kandala, Evidence for the utility of quantum computing before fault tolerance, *Nature* **618**, 500 (2023).
- [21] T. A. Chowdhury, K. Yu, M. A. Shamim, M. L. Kabir, and R. S. Sufian, Enhancing quantum utility: Simulating large-scale quantum spin chains on superconducting quantum computers, *Phys. Rev. Res.* **6**, 033107 (2024).
- [22] R. C. Farrell, M. Ila, A. N. Ciavarella, and M. J. Savage, Scalable circuits for preparing ground states on digital quantum computers: The Schwinger model vacuum on 100 qubits, *PRX Quantum* **5**, 020315 (2024).
- [23] M. Grossi, O. Kiss, F. De Luca, C. Zollo, I. Gremese, and A. Mandarino, Finite-size criticality in fully connected spin models on superconducting quantum hardware, *Phys. Rev. E* **107**, 024113 (2023).
- [24] O. Kiss, M. Grossi, and A. Roggero, Quantum error mitigation for Fourier moment computation (2024), [arXiv:2401.13048](https://arxiv.org/abs/2401.13048) [quant-ph].
- [25] Z. Cai, R. Babbush, S. C. Benjamin, S. Endo, W. J. Hugrins, Y. Li, J. R. McClean, and T. E. O'Brien, Quantum error mitigation, *Rev. Mod. Phys.* **95**, 045005 (2023).
- [26] L. Abdurakhimov, J. Adam, H. Ahmad, O. Ahoenen, M. Algaba, G. Alonso, V. Bergholm, R. Beriwai, M. Beuerle, C. Bockstiegel, *et al.*, Technology and performance benchmarks of iqm's 20-qubit quantum computer (2024), [arXiv:2408.12433](https://arxiv.org/abs/2408.12433) [quant-ph].
- [27] M. Born and V. Fock, Beweis des adiabatensatzes, *Zeitschrift für Physik* **51**, 165 (1928).

- [28] A. Miessen, P. J. Ollitrault, F. Tacchino, and I. Tavernelli, Quantum algorithms for quantum dynamics, *Nature Computational Science* **3**, 25 (2023).
- [29] M. Suzuki, Fractal decomposition of exponential operators with applications to many-body theories and monte carlo simulations, *Physics Letters A* **146**, 319 (1990).
- [30] A. M. Childs, Y. Su, M. C. Tran, N. Wiebe, and S. Zhu, Theory of Trotter error with commutator scaling, *Phys. Rev. X* **11**, 011020 (2021).
- [31] H. Zhao, M. Bukov, M. Heyl, and R. Moessner, Adaptive trotterization for time-dependent Hamiltonian quantum dynamics using piecewise conservation laws, *Phys. Rev. Lett.* **133**, 010603 (2024).
- [32] E. Campbell, Random compiler for fast Hamiltonian simulation, *Phys. Rev. Lett.* **123**, 070503 (2019).
- [33] O. Kiss, M. Grossi, and A. Roggero, Importance sampling for stochastic quantum simulations, *Quantum* **7**, 977 (2023).
- [34] D. W. Berry, A. M. Childs, Y. Su, X. Wang, and N. Wiebe, Time-dependent Hamiltonian simulation with L^1 -norm scaling, *Quantum* **4**, 254 (2020).
- [35] A. Rajput, A. Roggero, and N. Wiebe, Hybridized Methods for Quantum Simulation in the Interaction Picture, *Quantum* **6**, 780 (2022).
- [36] M. Kieferová, A. Scherer, and D. W. Berry, Simulating the dynamics of time-dependent Hamiltonians with a truncated Dyson series, *Physical Review A* **99**, 042314 (2019).
- [37] K. Sharma and M. C. Tran, Hamiltonian simulation in the interaction picture using the magnus expansion (2024), [arXiv:2404.02966 \[quant-ph\]](https://arxiv.org/abs/2404.02966).
- [38] P. A. M. Casares, M. S. Zini, and J. M. Arrazola, Quantum simulation of time-dependent Hamiltonians via commutator-free quasi-magnus operators (2024), [arXiv:2403.13889 \[quant-ph\]](https://arxiv.org/abs/2403.13889).
- [39] J. Watkins, N. Wiebe, A. Roggero, and D. Lee, Time dependent Hamiltonian simulation using discrete clock constructions (2022), [arXiv:2203.11353 \[quant-ph\]](https://arxiv.org/abs/2203.11353).
- [40] B. Shi and F. Mintert, Quantum simulations of time-dependent Hamiltonians beyond the quasistatic approximation, *Phys. Rev. Res.* **6**, 023097 (2024).
- [41] A. M. Childs, D. Maslov, Y. Nam, N. J. Ross, and Y. Su, Toward the first quantum simulation with quantum speedup, *Proceedings of the National Academy of Sciences* **115**, 9456 (2018).
- [42] F. Marxer, A. Vepsäläinen, S. W. Jolin, J. Tuorila, A. Landra, C. Ockeloen-Korppi, W. Liu, O. Ahonen, A. Auer, L. Belzane, V. Bergholm, C. F. Chan, K. W. Chan, T. Hiltunen, J. Hotari, E. Hyypä, J. Ikonen, D. Janzso, M. Koistinen, J. Kotilahti, T. Li, J. Luus, M. Papic, M. Partanen, J. Rabinä, J. Rosti, M. Savytskyi, M. Seppälä, V. Sevriuk, E. Takala, B. Tarasinski, M. J. Thapa, F. Tosto, N. Vorobeva, L. Yu, K. Y. Tan, J. Hassel, M. Möttönen, and J. Heinsoo, Long-distance transmon coupler with cz-gate fidelity above 99.8%, *PRX Quantum* **4**, 010314 (2023).
- [43] M. Urbanek, B. Nachman, V. R. Pascuzzi, A. He, C. W. Bauer, and W. A. de Jong, Mitigating depolarizing noise on quantum computers with noise-estimation circuits, *Phys. Rev. Lett.* **127**, 270502 (2021).
- [44] S. A Rahman, R. Lewis, E. Mendicelli, and S. Powell, Self-mitigating trotter circuits for SU(2) lattice gauge theory on a quantum computer, *Phys. Rev. D* **106**, 074502 (2022).
- [45] A. H. Z. Kavaki and R. Lewis, From square plaquettes to triamond lattices for SU(2) gauge theory, *Communications Physics* **7**, 208 (2024).
- [46] Z. Cai and S. Benjamin, Constructing smaller Pauli twirling sets for arbitrary error channels, *Sci Rep* **9**, 1128 (2019).
- [47] E. van den Berg, Z. K. Mineev, and K. Temme, Model-free readout-error mitigation for quantum expectation values, *Phys. Rev. A* **105**, 032620 (2022).
- [48] P. D. Nation, H. Kang, N. Sundaresan, and J. M. Gambetta, Scalable mitigation of measurement errors on quantum computers, *PRX Quantum* **2**, 040326 (2021).
- [49] D. Perez-Garcia, F. Verstraete, M. M. Wolf, and J. I. Cirac, Matrix product state representations, *Quantum Info. Comput.* **7**, 401–430 (2007).
- [50] L. Mead and N. Papanicolaou, Maximum entropy in the problem of moments, *Journal of Mathematical Physics* **25** (1984).
- [51] Y. Quek, D. S. França, S. Khatri, *et al.*, Exponentially tighter bounds on limitations of quantum error mitigation, *Nature Physics* **10.1038/s41567-024-02536-7** (2024).
- [52] R. Takagi, S. Endo, S. Minagawa, and M. Gu, Fundamental limits of quantum error mitigation, *npj Quantum Information* **8**, 114 (2022).
- [53] T. Schuster, C. Yin, X. Gao, and N. Y. Yao, A polynomial-time classical algorithm for noisy quantum circuits (2024), [arXiv:2407.12768 \[quant-ph\]](https://arxiv.org/abs/2407.12768).
- [54] A. Katarbwa, K. Gratsea, A. Caesura, and P. D. Johnson, Early fault-tolerant quantum computing, *PRX Quantum* **5**, 020101 (2024).
- [55] L. Lin and Y. Tong, Heisenberg-limited ground-state energy estimation for early fault-tolerant quantum computers, *PRX Quantum* **3**, 010318 (2022).
- [56] O. Kiss, U. Azad, B. Requena, A. Roggero, D. Wakeham, and J. M. Arrazola, Early fault-tolerant quantum algorithms in practice: Application to ground-state energy estimation (2024), [arXiv:2405.03754 \[quant-ph\]](https://arxiv.org/abs/2405.03754).
- [57] N. S. Blunt, L. Caune, R. Izsák, E. T. Campbell, and N. Holzmann, Statistical phase estimation and error mitigation on a superconducting quantum processor, *PRX Quantum* **4**, 040341 (2023).
- [58] F. J. Gómez-Ruiz, J. J. Mayo, and A. del Campo, Full counting statistics of topological defects after crossing a phase transition, *Phys. Rev. Lett.* **124**, 240602 (2020).
- [59] A. Hashim, R. K. Naik, A. Morvan, J.-L. Ville, B. Mitchell, J. M. Kreikebaum, M. Davis, E. Smith, C. Iancu, K. P. O'Brien, I. Hincks, J. J. Wallman, J. Emerson, and I. Siddiqi, Randomized compiling for scalable quantum computing on a noisy superconducting quantum processor, *Phys. Rev. X* **11**, 041039 (2021).
- [60] J. J. Wallman and J. Emerson, Noise tailoring for scalable quantum computation via randomized compiling, *Phys. Rev. A* **94**, 052325 (2016).
- [61] O. Kiss, M. Grossi, P. Lougovski, F. Sanchez, S. Vallecorsa, and T. Papenbrock, Quantum computing of the ${}^6\text{Li}$ nucleus via ordered unitary coupled clusters, *Phys. Rev. C* **106**, 034325 (2022).

Appendix A: Error mitigation

Error mitigation [25] is an essential tool to conduct experiments on near-term quantum computers without

error correction. In this work, we synergistically use different error suppression and mitigation techniques, which we describe below.

1. Noise renormalization

The workhorse of our error mitigation protocol is based on a noise renormalization technique, successfully used in [22, 24, 43–45]. The idea is to assume a noise model, estimate the corresponding parameters on the quantum device and reverse its effect in the post-processing stage. In the following, we shall assume a depolarising noise model $\mathcal{N}_p[\cdot]$ with parameter p , which maps the expectation value of a Pauli observable σ under a quantum state ρ to

$$\text{Tr}\{\sigma\mathcal{N}_p[\rho]\} = (1-p)\text{Tr}\{\sigma\rho\}. \quad (\text{A1})$$

If the parameter p is known, the results can be corrected by dividing the noisy results by $(1-p)$. The main idea is then to estimate $(1-p)$ by running a circuit with known expectation value. This becomes particularly simple when $h = 0$ or $th = \pi$. Hence in the first case the evolution of the field is the identity and in the second a uniform bit flip. In both cases, this action commutes with the interaction part, and we have

$$\langle \bar{\uparrow} | \mathcal{U}^\dagger(t) \hat{n} \mathcal{U}(t) | \bar{\uparrow} \rangle = 1, \quad (\text{A2})$$

where $|\bar{\uparrow}\rangle$ is the uniform superposition state obtained by applying a layer of Hadamard gates to $|0\rangle^{\otimes N}$. Since we require that the circuit is as close as the original one as possible, we choose the field at time t such as $h = \pi/t$. Even if the expectation values takes a simple form, the full circuit is still executed, enabling us to effectively estimate $(1-p)$ by evaluating Eq. A2. We note that, in practice, each component of \hat{n} are individually re-normalized.

2. Randomized compiling

The main assumption of the noise renormalization protocol is that the noise is depolarising. However, this is not the case on real quantum devices. To alleviate this effect, the circuits are randomly compiled [59]. In practice, each two-qubit gate is twirled using single-qubit Pauli rotation, chosen in such a way that the transformed and original circuits are equivalent. This process is known as Pauli twirling [46] and effectively turns the noise channel into a Pauli channel. Moreover, under twirling, the noise accumulates as in a random walk [60], which is quadratically slower than it would add coherently. Since the data obtained in this process are merged together before computing expectation values, we can simply distribute the shot budget over all the twirls, thus avoiding an increase in the number of samples.

Twirling can also be used to mitigate measurement errors [47] in the computation of expectation values. This process is performed by randomly flipping the state of

the qubit before measurement, and reverse the value of the measured bit, if applicable. effectively, measurement twirling diagonalise the readout transfer-matrix, making it easier to invert using techniques describe below.

3. Readout error mitigation

We mitigate readout errors by calibrating the device. Since a full calibration is exponentially expensive, we adopt a sparse strategy [48, 61] by only measuring the N -qubit state $|0\rangle^{\otimes N}$ and $|1\rangle^{\otimes N}$, and build the confusion matrices

$$P_k = \begin{pmatrix} P_{0,0}^{(k)} & P_{0,1}^{(k)} \\ P_{1,0}^{(k)} & P_{1,1}^{(k)} \end{pmatrix}, \quad (\text{A3})$$

where, $P_{i,j}^{(k)}$ is the probability of the k -th qubit to be in $|j\rangle$ while measured in $|i\rangle$, for $i, j \in \{0, 1\}$. The measurements \vec{M}^k of the qubit k is later corrected as

$$\vec{M}_{\text{corrected}}^k = (P_k)^{-1} \vec{M}^k. \quad (\text{A4})$$

As stated above, measurement twirling is performed to diagonalize the transfer-matrix, thus making it easier to invert.

Appendix B: Propagation of statistical uncertainties

$$P_b(m; p) = \binom{M}{m} p^m (1-p)^{(M-m)}. \quad (\text{B1})$$

The probability p of obtaining $|1\rangle$ is then inferred with Bayes theorem

$$P(p|m_i) = \frac{P(m_i|p)P(p)}{\int dq P(m_i|q)P(q)}, \quad (\text{B2})$$

which is given in closed form by the beta prior

$$P_\beta(p; \alpha, \beta) = \frac{\Gamma(\alpha + \beta)}{\Gamma(\alpha)\Gamma(\beta)} p^{(\alpha-1)} (1-p)^{(\beta-1)}. \quad (\text{B3})$$

Here, $\alpha, \beta > 0$ parameterize the beta distribution and represent the number of times the basis vector i is measured. Note that we only sample from binary string appearing at least once in the data, to avoid sampling from exponentially many terms. After this inference phase, the following procedure can be used to determine the expected values: (i) sample a value p'_k from the posterior $P(p'_k|m_i)$. (ii) sample L new measurements from the likelihood $P_b(m'_k; p'_k)$. (iii) Compute expectations values by averaging over the generate measurements. To generalized to multiple qubits, we can use the Dirichlet distribution, which is a closed-form prior for a multinomial distribution.